# Robust output-feedback stabilization for incompressible flows using low-dimensional $\mathcal{H}_\infty$-controllers

Peter Benner[*]    Jan Heiland[†]    Steffen W. R. Werner[‡]

[*]*Max Planck Institute for Dynamics of Complex Technical Systems, Sandtorstraße 1, 39106 Magdeburg, Germany.* Email: benner@mpi-magdeburg.mpg.de, ORCID: 0000-0003-3362-4103

*Otto von Guericke University Magdeburg, Faculty of Mathematics, Universitätsplatz 2, 39106 Magdeburg, Germany.* Email: peter.benner@ovgu.de

[†]*Max Planck Institute for Dynamics of Complex Technical Systems, Sandtorstraße 1, 39106 Magdeburg, Germany.* Email: heiland@mpi-magdeburg.mpg.de, ORCID: 0000-0003-0228-8522

*Otto von Guericke University Magdeburg, Faculty of Mathematics, Universitätsplatz 2, 39106 Magdeburg, Germany.* Email: jan.heiland@ovgu.de

[‡]*Max Planck Institute for Dynamics of Complex Technical Systems, Sandtorstraße 1, 39106 Magdeburg, Germany.* Email: werner@mpi-magdeburg.mpg.de, ORCID: 0000-0003-1667-4862

Output-based controllers are known to be fragile with respect to model uncertainties. The standard $\mathcal{H}_\infty$-control theory provides a general approach to robust controller design based on the solution of the $\mathcal{H}_\infty$-Riccati equations. In view of stabilizing incompressible flows in simulations, two major challenges have to be addressed: the high-dimensional nature of the spatially discretized model and the differential-algebraic structure that comes with the incompressibility constraint. This work demonstrates the synthesis of low-dimensional robust controllers with guaranteed robustness margins for the stabilization of incompressible flow problems. The performance and the robustness of the reduced-order controller with respect to linearization and model reduction errors are investigated and illustrated in numerical examples.

**Keywords:** robust control, incompressible flows, stabilizing feedback controller

## 1 Introduction

We consider the incompressible Navier-Stokes equations with inputs and outputs

$$\dot{v} = -(v \cdot \nabla)v + \frac{1}{\mathsf{Re}}\Delta v - \nabla p + \mathcal{B}u, \tag{1a}$$

$$0 = \nabla \cdot v, \tag{1b}$$

$$y = \mathcal{C}v, \tag{1c}$$

and the question when a linear output-feedback controller $\mathcal{K}\colon y \mapsto u$ can stabilize this nonlinear system around a possibly unstable steady state in the presence of system uncertainties. Here, the variables $v$ and $p$ describe the evolution of the velocity and pressure fields in a given flow setup that is parametrized through the Reynolds number $\mathsf{Re}$. The operator $\mathcal{B}$ models the actuation through the controls, and $\mathcal{C}$ is the output operator.

---

We will approach this question through a semi-discrete and linearized approximation to (1), model order reduction to cope with the high dimensionality of the controller design problem, and the design of controllers that can compensate for a large class of system uncertainties. Basically, our argument is that discretization and model reduction errors are of the same nature so that a proven robustness margin can possibly overcome unmodeled uncertainties, too.

Anyways, in order to potentially work in physical setups, any model-based controller needs a certain robustness against inevitable model errors. This rules out the standard LQG-design that has no guaranteed stability margin [21]. A general remedy is provided by $\mathcal{H}_\infty$-controllers that, provably, can compensate for linearization errors [8, 28], discretization errors [9, 18], and truncation errors [36].

The $\mathcal{H}_\infty$-theory roots in the 1980s [45]; see also [22, 23] for the historical background. In view of its application in simulations, the development of state space formulations [20, 23] meant a breakthrough since it came with general formulas for the controller design based on the solutions of indefinite Riccati equations. Nonetheless, the computational effort for solving these Riccati equations is significant so that, up to now, this design approach has rarely been considered in large-scale simulations let alone the case where algebraic constraints are present, that is for *differential-algebraic equations* (DAEs) or *descriptor systems*.

If one leaves aside the *offline* effort for designing the controller, the theory seems well suited for large-scale problems since the controllers allow for a low-dimensional approximation with a-priori estimates on performance and robustness [36]. The involved reduction is based on *balanced truncation* and has been investigated for descriptor systems in [35].

Thus, with flow control in mind, the solution of large-scale Riccati equations related to DAEs enables the use of the general $\mathcal{H}_\infty$-theory.

It has been acknowledged that for general DAE systems, the standard symmetric Riccati equations are only suitable under very restrictive conditions [6]. A nonsymmetric version has been shown to provide a true generalization for the $\mathcal{H}_\infty$-controller [11] to the *index-1* case and is widely applicable for LQG-design for *impulse controllable* descriptor systems [30, 42].

In this work, we consider the incompressible Navier-Stokes equations with control inputs in the momentum equation and velocity measurements only, so that the input-to-output behavior can be equivalently realized as an ODE. Still, we keep the DAE structure since the corresponding transformation will not be available in practice. Then, the challenge is to realize what is suggested by the ODE theory without explicitly resorting to transformations and projections. For that, we adapt the established technique [2, 27, 31, 43] of realizing the projections through the solution of saddle-point systems, so that structure and sparsity preserved during all operations.

The $\mathcal{H}_\infty$-feedback control for the 2D incompressible Navier-Stokes equations has been treated in [19] from a theoretical perspective. There, unmodeled boundary inputs are considered and existence of optimal feedback solutions is shown with the help of Riccati equations. The general $\mathcal{H}_\infty$-control problem is discussed in [3, Ch. 5]. Here, summing up the relevant research, the established state space theory is adapted to the infinite-dimensional incompressible Navier-Stokes equations.

In this paper, we explore the Riccati-based $\mathcal{H}_\infty$-controller design for spatially discretized two-dimensional incompressible flows. To this end,

- we adapt the theory for the implicit treatment of the incompressibility constraint to the $\mathcal{H}_\infty$-optimization problem,

- we leverage $\mathcal{H}_\infty$-balanced truncation to reduce the dimension of the controller design problem,

- we provide numerically accessible formulas for a-priori estimation of the robustness of the controller with respect to the $\mathcal{H}_\infty$-balanced truncation model reduction error as well as linearization errors, and

- illustrate the performance in two challenging numerical examples.

As a result, we provide a complete numerical approach that makes $\mathcal{H}_\infty$-controller design feasible for large-scale Navier-Stokes systems and provides computable bounds on the robustness of the performance with respect to both linearization errors [12] and model reduction errors [36]. The situation

that the controller is based on inexact linearizations is relevant in applications and fits well into the presented framework; cp. [9, 12, 28].

The presented numerical studies are based on the popular setup of the two-dimensional wake behind a cylinder; see [16, 25, 26, 37, 44] for examples.

This paper is organized as follows: In Section 2, we introduce the concepts of $\mathcal{H}_\infty$-controller design and truncation via the solution of Riccati equations and how the theory extends to semi-discretized incompressible Navier-Stokes equations. In Section 3, we derive the low-rank iteration for the solution of the Riccati equation that implicitly respects the incompressibility constraint and provide the formulas for the order-reduced robust controller. By means of two flow setups, we report on the performance both of the solution approach and the resulting controller in Section 4.

## 2 Mathematical basics

In this section, we introduce the basic concept and state-space approach of robust $\mathcal{H}_\infty$-controller design and how the relevant formulas are realized for incompressible flow control setups.

### 2.1 Riccati-based $\mathcal{H}_\infty$ controller design

For practical applications, the design of controllers that provide a certain robustness against disturbances is essential, as neither models nor numerical computations are fully able to match reality. The $\mathcal{H}_\infty$-controller theory provides the design of such controllers. In general, linear time-invariant systems of the form

$$E\dot{x}(t) = Ax(t) + B_1 w(t) + B_2 u(t), \tag{2a}$$
$$z(t) = C_1 x(t) + D_{11} w(t) + D_{12} u(t), \tag{2b}$$
$$y(t) = C_2 x(t) + D_{21} w(t) + D_{22} u(t), \tag{2c}$$

with $E, A \in \mathbb{R}^{n \times n}$, $B_1 \in \mathbb{R}^{n \times m_1}$, $B_2 \in \mathbb{R}^{n \times m_2}$, $C_1 \in \mathbb{R}^{p_1 \times n}$, $C_2 \in \mathbb{R}^{p_2 \times n}$, $D_{11} \in \mathbb{R}^{p_1 \times m_1}$, $D_{12} \in \mathbb{R}^{p_1 \times m_2}$, $D_{21} \in \mathbb{R}^{p_2 \times m_1}$, and $D_{22} \in \mathbb{R}^{p_2 \times m_2}$, are considered. In (2), the internal states $x$ are influenced by the control inputs $u$ and disturbances $w$, and the user can observe the measurements $y$ and performance outputs $z$ of the system. The basic aim is to find a feedback controller $K\colon y \mapsto u$ that internally stabilizes (2). Considering (2) in frequency domain allows the formulation of the system's input-to-output relation in terms of its (partitioned with respect to the different inputs and outputs) transfer function

$$G(s) = \begin{bmatrix} C_1 \\ C_2 \end{bmatrix} (sE - A)^{-1} \begin{bmatrix} B_1 & B_2 \end{bmatrix} + \begin{bmatrix} D_{11} & D_{12} \\ D_{21} & D_{22} \end{bmatrix} =: \begin{bmatrix} G_{11}(s) & G_{12}(s) \\ G_{21}(s) & G_{22}(s) \end{bmatrix}.$$

Let also $K(s)$ denote the transfer function of the controller $K$, the disturbance-to-performance behavior of the system can be formulated as

$$Z(s) = (G_{11}(s) + G_{12}(s)K(s)(I - G_{22}(s)K(s))^{-1}G_{21}(s))W(s) =: \mathcal{F}(G, K)W(s), \tag{3}$$

where $Z$, $W$ are the Laplace transforms of the performances and disturbances, and $I$ denotes the identity matrix of appropriate size. $\mathcal{F}$ is a *lower linear fractional transformation*. With (3), the *optimal $\mathcal{H}_\infty$-control problem* is to find a controller $K$ that solves

$$\min_{K \text{ stabilizing}} \|\mathcal{F}(G, K)\|_{\mathcal{H}_\infty} =: \gamma_{\mathsf{opt}}, \tag{4}$$

where $\|.\|_{\mathcal{H}_\infty}$ is the $\mathcal{H}_\infty$-norm. In general, this optimization problem (4) is too difficult to solve. Instead, one can consider a relaxation in terms of the *sub-optimal $\mathcal{H}_\infty$-control problem*: Find a stabilizing controller $K$ such that

$$\|\mathcal{F}(G, K)\|_{\mathcal{H}_\infty} < \gamma; \tag{5}$$

which is then solved successively for decreasing robustness margins $\gamma \to \gamma_{\mathsf{opt}}$.

A state-space theory has been developed that provides formulas for such suboptimal controllers. For ease of notation and theoretical derivations, we use the following set of (classical) assumptions:

1. $E$ is invertible,

2. $D_{11}, D_{22} = 0$,

3. $(sE - A, B_1)$ is stabilizable and $(sE - A, C_1)$ is detectable,

4. $(sE - A, B_2)$ is stabilizable and $(sE - A, C_2)$ is detectable,

5. $D_{12}^\mathsf{T} \begin{bmatrix} C_1 & D_{12} \end{bmatrix} = \begin{bmatrix} 0 & I \end{bmatrix}$, and $\begin{bmatrix} B_1 \\ D_{21} \end{bmatrix} D_{21}^\mathsf{T} = \begin{bmatrix} 0 \\ I \end{bmatrix}$.

Given a $\gamma > \gamma_{\mathsf{opt}}$, there exists an admissible controller $K$ if and only if there exist unique stabilizing solutions $X_{\mathcal{H}_\infty}, Y_{\mathcal{H}_\infty}$ to the regulator and filter $\mathcal{H}_\infty$-Riccati equations

$$A^\mathsf{T} X E + E^\mathsf{T} X A - E^\mathsf{T} X (B_2 B_2^\mathsf{T} - \gamma^{-2} B_1 B_1^\mathsf{T}) X E + C_1^\mathsf{T} C_1 = 0, \tag{6a}$$

$$A Y E^\mathsf{T} + E Y A^\mathsf{T} - E Y (C_2^\mathsf{T} C_2 - \gamma^{-2} C_1^\mathsf{T} C_1) Y E^\mathsf{T} + B_1 B_1^\mathsf{T} = 0; \tag{6b}$$

and, additionally,

$$\gamma^2 > \lambda_{\max}(Y_{\mathcal{H}_\infty} E^\mathsf{T} X_{\mathcal{H}_\infty} E) \tag{7}$$

holds; see, e.g., [20, 46]. Then a stabilizing controller solving (5) is known in the literature as the *central or minimum entropy controller*, given via

$$K : \begin{cases} \widetilde{E} \dot{\tilde{x}}(t) = \widetilde{A} \tilde{x}(t) + \widetilde{B} y(t), \\ u(t) = \widetilde{C} \tilde{x}(t), \end{cases}$$

where the system matrices can be computed as

$$\begin{aligned} \widetilde{E} &= E, \\ \widetilde{A} &= A + E Y_{\mathcal{H}_\infty} (\gamma^{-2} C_1^\mathsf{T} C_1 - C_2^\mathsf{T} C_2) - B_2 B_2^\mathsf{T} X_{\mathcal{H}_\infty} E Z_{\mathcal{H}_\infty}, \\ \widetilde{B} &= E Y_{\mathcal{H}_\infty} C_2^\mathsf{T}, \\ \widetilde{C} &= -B_2^\mathsf{T} X_{\mathcal{H}_\infty} E Z_{\mathcal{H}_\infty}, \end{aligned} \tag{8}$$

with $Z_{\mathcal{H}_\infty} = (I_n - \gamma^{-2} Y_{\mathcal{H}_\infty} E^\mathsf{T} X_{\mathcal{H}_\infty} E)^{-1}$; cp. [20, Sec. III.C] for the general case and also [36, Eqns. (16) and (17)] for the normalized case described in the following chapter.

## 2.2 The normalized $\mathcal{H}_\infty$ problem and low-rank robust controllers

The target application of this work is output-based feedback control of a nonlinear system that is robust against system uncertainties stemming from linearization and reduction errors. As a general model for the linearization uncertainty, we will assume that the system matrix $A$ is subjected to an additive perturbation. In this case, in a feedback arrangement, disturbance inputs will be induced by the measurements of the perturbed state and enter the system as a perturbation of the control input. Accordingly, in (2), one can consider $B_1 = B_2 =: B$ and $C_1 = C_2 =: C$ which leads to the so-called *normalized $\mathcal{H}_\infty$-control problem*.

A $\mathcal{H}_\infty$-robust controller based on the *normalized* problem then applies in our context as follows. First, its robustness margin $\gamma$ can be weighed up against the system error that arises from truncating certain states of the controller. Since a full-order controller would be of the same size as the system, such a truncation significantly supports the efficient evaluation of the feedback law during a simulation.

Second, the robustness can cover the system error that comes from an inaccurate linearization. In this section, we discuss both application scenarios and provide relevant a-priori and a-posteriori estimates.

As for controller truncation we consider the $\mathcal{H}_\infty$-balanced truncation approach as it has been reported in [36]. For that we introduce another special case of (2), namely the so-called *normalized linear-quadratic Gaussian* system

$$
\begin{aligned}
E\dot{x}(t) &= Ax(t) + Bw_1(t) + Bu(t),\\
z_1(t) &= Cx(t),\\
z_2(t) &= u(t),\\
y(t) &= Cx(t) + w_2(t).
\end{aligned}
\tag{9}
$$

Apart from assuming $B_1 = B_2 =: B$ and $C_1 = C_2 =: C$, system (9) differs from (2) in so far as it defines disturbance inputs and performance outputs in a way that satisfies the fundamental assumptions on the feed-through terms listed in Section 2.1. In general, the assumptions on the structure of (9) are either needed for well-posedness of the control problem or readily achieved by state and control space transformations; cp. [46, Ch. 17.3]. For our intended application these assumptions pose no restriction at all.

With these assumptions on (9), it has been shown (see, e.g., [46, Thm. 16.4]) that the existence of an admissable controller that solves the $\mathcal{H}_\infty$-control problem for the suboptimal gain $\gamma$ (cp. (5)), implies the existence of positive semi-definite matrices $X_{\mathcal{H}_\infty}$ and $Y_{\mathcal{H}_\infty}$ that solve

$$
AY_{\mathcal{H}_\infty}E^\mathsf{T} + EY_{\mathcal{H}_\infty}A^\mathsf{T} - (1 - \gamma^{-2})EY_{\mathcal{H}_\infty}C^\mathsf{T}CY_{\mathcal{H}_\infty}E^\mathsf{T} + BB^\mathsf{T} = 0,
\tag{10a}
$$
$$
A^\mathsf{T}X_{\mathcal{H}_\infty}E + E^\mathsf{T}X_{\mathcal{H}_\infty}A - (1 - \gamma^{-2})E^\mathsf{T}X_{\mathcal{H}_\infty}BB^\mathsf{T}X_{\mathcal{H}_\infty}E + C^\mathsf{T}C = 0,
\tag{10b}
$$

such that the the spectrum condition (7) holds and such that the matrix pencils $sE - (A - (1 - \gamma^{-2})EY_{\mathcal{H}_\infty}C^\mathsf{T}C)$ and $sE - (A - (1 - \gamma^{-2})BB^\mathsf{T}X_{\mathcal{H}_\infty}E)$ are stable.

By means of the two matrices $X_{\mathcal{H}_\infty}$ and $Y_{\mathcal{H}_\infty}$, a so-called $\mathcal{H}_\infty$-balanced transformation of the system can be computed [36, Prop. 4.10] that enables a truncation systems or controller states with an a-priori control on the approximation error.

A practical implementation of this $\mathcal{H}_\infty$-Balanced Truncation (HINFBT) for large-scale systems is laid in Algorithm 1 that uses *square root balancing approach* on approximating low-rank factorizations of $X_{\mathcal{H}_\infty}$ and $Y_{\mathcal{H}_\infty}$. An implementation of Algorithm 1 for the dense system case can also be found in [15].

An error bound is given in terms of a normalized coprime factorization of the system: Let $G(s) = M(s)^{-1}N(s)$ and $\widehat{G}(s) = \widehat{M}(s)^{-1}\widehat{N}(s)$ be a normalized left coprime factorizations of the original system $G$ and the reduced-order model $\widehat{G}$ obtained by HINFBT, then

$$
\left\| \begin{bmatrix} \beta(N - \widehat{N}) & M - \widehat{M} \end{bmatrix} \right\|_{\mathcal{H}_\infty} \leq 2 \sum_{k=r+1}^{n} \frac{\beta\sigma_k}{\sqrt{1 + \beta^2\sigma_k^2}}
\tag{11}
$$

holds, with $\beta = \sqrt{1 - \gamma^{-2}}$ and $\sigma_k$, the characteristic $\mathcal{H}_\infty$-values, which are given as the positive square roots of the eigenvalues of $Y_{\mathcal{H}_\infty}E^\mathsf{T}X_{\mathcal{H}_\infty}E$.

More importantly, the robustness margin $\gamma$ can be put in context with the truncation error in the controller so that one can estimate how large the reduced-order controller needs to be to still stabilize the original system.

Let again $G(s) = M(s)^{-1}N(s)$ and $\widehat{G}(s) = \widehat{M}(s)^{-1}\widehat{N}(s)$ be the normalized left coprime factorizations of the original system and the reduced-order approximation computed by HINFBT, and

$$
\beta\hat{\epsilon} := \left\| \begin{bmatrix} \beta(N - \widehat{N}) & M - \widehat{M} \end{bmatrix} \right\|_{\mathcal{H}_\infty}
$$

---

**Algorithm 1:** (Approximate) $\mathcal{H}_\infty$-balanced truncation square root method.

**Input:** $A, B, C, E$ from (9), robustness margin $\gamma > 0$.

**Output:** Matrices of the reduced-order system $\widehat{A}, \widehat{B}, \widehat{C}, \widehat{E}$.

**1** Compute low-rank approximations $Y_{\mathcal{H}_\infty} \approx RR^\mathsf{T}$ and $X_{\mathcal{H}_\infty} \approx LL^\mathsf{T}$ to the unique stabilizing solutions of (10).

**2** Compute the singular value decomposition

$$L^\mathsf{T} E R = \begin{bmatrix} U_1 & U_2 \end{bmatrix} \begin{bmatrix} \Sigma_1 & \\ & \Sigma_2 \end{bmatrix} \begin{bmatrix} V_1^\mathsf{T} \\ V_2^\mathsf{T} \end{bmatrix},$$

with $\Sigma_1 = \operatorname{diag}(\sigma_1, \ldots, \sigma_r)$ containing the $r$ largest characteristic $\mathcal{H}_\infty$-values.

**3** Construct the truncation matrices

$$W = LU_1 \Sigma_1^{-\frac{1}{2}} \quad \text{and} \quad T = RV_1 \Sigma_1^{-\frac{1}{2}}.$$

**4** Compute the reduced-order model by

$$\widehat{E} = W^\mathsf{T} E T = I_r, \quad \widehat{A} = W^\mathsf{T} A T, \quad \widehat{B} = W^\mathsf{T} B, \quad \widehat{C} = CT.$$

---

to be the scaled coprime factor error, with $\beta = \sqrt{1 - \gamma^{-2}}$. Then, a sufficient condition for the reduced-order central controller $\widehat{K}$ associated with $\widehat{G}$ to stabilize the original system $G$ is

$$\hat{\epsilon}(\beta + \hat{\gamma}) < 1, \tag{12}$$

where $\hat{\gamma} = \|\mathcal{F}(\widehat{G}, \widehat{K})\|_{\mathcal{H}_\infty}$; see [36, Cor. 5.5]. As a practical alternative to (12) which can only be evaluated after the computation of the reduced-order model, an a-priori estimate can be derived based on the HINFBT error bound (11)

$$\beta\epsilon := 2 \sum_{k=r+1}^{n} \frac{\beta\sigma_k}{\sqrt{1 + \beta^2 \sigma_k^2}},$$

or more precisely

$$\epsilon = 2 \sum_{k=r+1}^{n} \frac{\sigma_k}{\sqrt{1 + \beta^2 \sigma_k^2}}.$$

With $\hat{\gamma} < \gamma$, where $\gamma$ was used as robustness margin in HINFBT, and $\hat{\epsilon} \leq \epsilon$, a sufficient a-priori condition for stabilization of the full-order system by the reduced-order central controller is

$$\epsilon(\beta + \gamma) < 1. \tag{13}$$

Note that, if the above estimates are fulfilled, the truncation preserves the stability but increases the disturbance to performance output gain. In fact, while the full-order *central controller* (8) for fulfills $\|\mathcal{F}(G, K)\|_{\mathcal{H}_\infty} < \gamma$, for the reduced order controller it only holds that

$$\|\mathcal{F}(G, \widehat{K})\|_{\mathcal{H}_\infty} \leq \hat{\gamma} + \frac{\hat{\epsilon}(1 + \hat{\gamma})(1 + \beta + \hat{\gamma})}{1 - \hat{\epsilon}(\beta + \hat{\gamma})} < \gamma + \frac{\epsilon(1 + \gamma)(1 + \beta + \gamma)}{1 - \epsilon(\beta + \gamma)}; \tag{14}$$

cp. [36].

As said, a second purpose of a robustness margin $\gamma$ is to ensure stability in the closed-loop system in the presence of system uncertainties. Generally, for any stabilizing controller $K$ that solves the

---

sub-optimal $\mathcal{H}_\infty$-controller problem (5) for the system $G(s) = M(s)^{-1}N(s)$ and robustness margin $\gamma$, it holds that (see, e.g., [34, Cor. 3.7]), that $K$ to stabilizes also the disturbed system $G_\Delta(s) = M_\Delta(s)^{-1}N_\Delta(s)$ if

$$\left\| \begin{bmatrix} N - N_\Delta & M - M_\Delta \end{bmatrix} \right\|_{\mathcal{H}_\infty} < \gamma^{-1}. \tag{15}$$

In view of stabilizing incompressible Navier-Stokes equations by linear feedback controllers, the following considerations are relevant with respect to the estimate (15). It has been shown that an error in the linearization used for controller design, smoothly transfers to a coprime factor perturbation in the transfer function; see [8, 28]. Accordingly, with increasing accuracy in the computation of the linearization, the difference becomes arbitrarily small so that, eventually, a robust controller based on a numerically computed linearization will be able to stabilize the system.

## 2.3 Semi-discretization and linearization of NSE

Next, we briefly illustrate how a linear finite dimensional ODE system can be derived as a base for the controller design for the nonlinear incompressible Navier-Stokes equations. Details of the discretization and the modeling of boundary control will be discussed together with the numerical examples in Section 4.

A Finite Elements discretization of the incompressible Navier-Stokes equations (1) leads to the semi-discrete system:

$$E\dot{v} = A_{\mathsf{S}}v + F(v) + J^{\mathsf{T}}p + Bu + f, \tag{16a}$$

$$0 = Jv + g, \tag{16b}$$

$$y = Cv, \tag{16c}$$

where $A_{\mathsf{S}}$ is the discrete approximation of $\frac{1}{\mathsf{Re}}\Delta$, $F$ models the convection, $J$ and $J^{\mathsf{T}}$ represent the discrete divergence and gradient, $B$ and $C$ are the discretized input and output operators, and where $f$ and $g$ are the inhomogeneities that arise from the inclusion of the inflow boundary condition in strong form. Let $v_\infty$ be the steady state with $u = 0$ so that with $v_\delta = v - v_\infty$ and $A^{(\infty)} := A_{\mathsf{S}} + (\partial_v F)(v_\infty)$,

$$E\dot{v_\delta} = A^{(\infty)}v_\delta + J^{\mathsf{T}}p + Bu, \tag{17a}$$

$$0 = Jv_\delta, \tag{17b}$$

$$y_\delta = Cv_\delta, \tag{17c}$$

provides a linearization that can be used for regulating the deviation $v_\delta$ and, thus, for designing a controller for stabilizing $v_\infty$. With the assumption that the chosen Finite Elements scheme is *LBB* stable, one can define a discrete realization of the *Leray* projector

$$\Pi^{\mathsf{T}} := I - E^{-1}J^{\mathsf{T}}(JE^{-1}J^{\mathsf{T}})J \tag{18}$$

that maps $v(t)$ into the kernel of $J$ along the orthogonal complement (in the inner product induced by the mass matrix $E$) of $J^{\mathsf{T}}$. Making use of $\Pi$ and the identities $\Pi E = E\Pi^{\mathsf{T}}$ – which holds for symmetric $E$ – and $\Pi^{\mathsf{T}}v_\delta = v_\delta$, we can eliminate the discrete pressure $p$ and the algebraic constraint $0 = Jv_\delta$ and rewrite (17) as an ODE

$$E\dot{v_\delta} = \Pi A^{(\infty)}\Pi^{\mathsf{T}}v_\delta + \Pi Bu \tag{19a}$$

$$y_\delta = C\Pi^{\mathsf{T}}v_\delta \tag{19b}$$

For such a realization in terms of an ODE, an $\mathcal{H}_\infty$-robust controller can be defined via the solutions to the projected $\mathcal{H}_\infty$-Riccati equations

$$\Pi A^{\mathsf{T}}\Pi^{\mathsf{T}}XE + E^{\mathsf{T}}X\Pi A\Pi^{\mathsf{T}} - (1 - \gamma^{-2})E^{\mathsf{T}}X\Pi BB^{\mathsf{T}}\Pi^{\mathsf{T}}XE + \Pi C^{\mathsf{T}}C\Pi^{\mathsf{T}} = 0, \tag{20a}$$

$$\Pi A\Pi^{\mathsf{T}}YE^{\mathsf{T}} + EY\Pi A^{\mathsf{T}}\Pi^{\mathsf{T}} - (1 - \gamma^{-2})EY\Pi C^{\mathsf{T}}C\Pi^{\mathsf{T}}YE^{\mathsf{T}} + \Pi BB^{\mathsf{T}}\Pi^{\mathsf{T}} = 0; \tag{20b}$$

Here, we have ignored the symmetry of $E$ in (19) in order to be in line with the general formulas (6).

In the context of nonlinear flow control problems, the problem of linearization errors and compensation by reduced-order controllers was considered in [12]. There it was mentioned that linearization errors in (17) from (16) result in additive disturbances on the transfer function, which can be handled as disturbances in the coprime factorization.

In view of numerical realizations, we note the left coprime factorizations for linear flow problems of the form (17) can be constructed as

$$\begin{bmatrix} N(s) & M(s) \end{bmatrix} = \mathcal{C}(s\mathcal{E} - \mathcal{A})^{-1} \begin{bmatrix} \mathcal{B} & -\mathcal{L} \end{bmatrix} + \begin{bmatrix} 0 & I_p \end{bmatrix},$$

where

$$\mathcal{E} = \begin{bmatrix} E & 0 \\ 0 & 0 \end{bmatrix}, \quad \mathcal{A} = \begin{bmatrix} A^{(\infty)} - (1 - \gamma^{-2})EY_{\mathcal{H}_\infty}C^\mathsf{T}C & J^\mathsf{T} \\ J & 0 \end{bmatrix},$$

$$\mathcal{C} = \begin{bmatrix} C & 0 \end{bmatrix}, \quad \mathcal{B} = \begin{bmatrix} B \\ 0 \end{bmatrix}, \quad \mathcal{L} = \begin{bmatrix} (1 - \gamma^{-2})EY_{\mathcal{H}_\infty}C^\mathsf{T} \\ 0 \end{bmatrix},$$

and with $Y_{\mathcal{H}_\infty}$ the stabilizing solution of (20); cp. [12], This representation makes the explicit computation of disturbances on the coprime factorizations, e.g., for the evaluation of the necessary robustness as in (15), accessible to numerical simulations.

## 3 Numerical methods

### 3.1 Projector-free realization for incompressible flows

In theory, the projected Riccati equations (20) can be treated with by iterative low-rank solvers [7, 14, 33, 40, 41, 43]. In practice, however, the use of the projector $\Pi$ as defined in (18) is not feasible, since its computation is time and memory consuming, and since an inaccurate version will introduce a systematic error. Therefore, like in many similar applications (see, e.g., [2, 24, 27]), we derive a suitable implicit realization of the projection as it was proposed initially in [31].

For that, we note that only the projected parts $X_\Pi := \Pi^\mathsf{T} X \Pi$ and $Y_\Pi = \Pi^\mathsf{T} Y \Pi$ of the Riccati solutions $X$ and $Y$ contribute to the controller (cp. (8) and [10]) and that $X_\Pi$ and $Y_\Pi$ solve the equations

$$\Pi A^\mathsf{T} \Pi^\mathsf{T} X_\Pi E^\mathsf{T} + E X_\Pi \Pi A \Pi^\mathsf{T} - (1 - \gamma^{-2})E X_\Pi B B^\mathsf{T} X_\Pi E^\mathsf{T} + \Pi C^\mathsf{T} C \Pi^\mathsf{T} = 0, \tag{21a}$$

$$\Pi A \Pi^\mathsf{T} Y_\Pi E + E^\mathsf{T} Y_\Pi \Pi A^\mathsf{T} \Pi^\mathsf{T} - (1 - \gamma^{-2})E^\mathsf{T} Y_\Pi C^\mathsf{T} C Y_\Pi E + \Pi B B^\mathsf{T} \Pi^\mathsf{T} = 0 \tag{21b}$$

that are derived from (20) by pre- and postmultiplication by $\Pi$ and $\Pi^\mathsf{T}$, respectively, and by means of the identities $\Pi^2 = \Pi$ and $\Pi E = E\Pi^\mathsf{T}$.

In computational methods for large-scale Riccati equations, low-rank factors $Z_k$ for $X \approx Z_k Z_k^\mathsf{T}$ are computed by repeated solves of shifted linear systems that for $X_\Pi$ read like

$$(\Pi A \Pi^\mathsf{T} + p_i E)Z_{k+1} = Z_k,$$

which with the requirement that $Z_k = \Pi^\mathsf{T} Z_k$ can be equivalently formulated as

$$\begin{bmatrix} A + p_i E & J^\mathsf{T} \\ J & 0 \end{bmatrix} \begin{bmatrix} Z_{k+1} \\ Z_\perp \end{bmatrix} = \begin{bmatrix} E^\mathsf{T} Z_k \\ 0 \end{bmatrix}.$$

Here, the complex scalar $p_i$ is a shift parameter that usually occurs in ADI or Krylov subspace based solvers and $Z_\perp$ is an auxiliary variable.
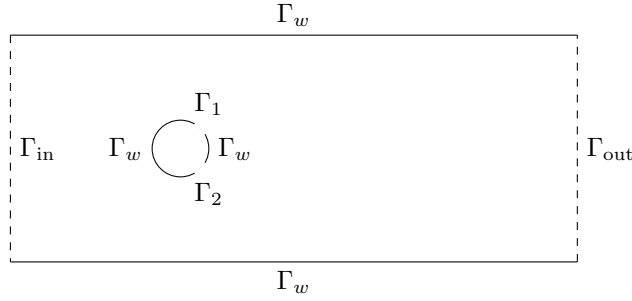
Figure 1: Computational domain of the cylinder wake.

## 3.2 Computation of low-rank controllers

The practical construction of a reduced-order controller for (16) follows, in principle, the different steps mentioned in this paper so far with some additional numerical tricks. For simplicity, we give a final summary of the performed steps in the following:

*Step 1. Computation of a suitable robustness margin:* So far, the margin $\gamma$ was assumed to be given, but in fact it can be computed utilizing the necessary and sufficient conditions for the existence of a stabilizing controller $K$ that solves (5). In practice, one solves repeatedly (20) for different instances of the robustness margin and uses (7) to determine the next iterate. Thereby, a sufficient $\gamma$ can be computed.

*Step 2. Construction of the reduced-order model:* Now, the original system (16) needs to be reduced by Algorithm 1. Therefore, we use the final solution factors to the projected algebraic Riccati equations (21) $Z_k^{\mathsf{r}}$ and $Z_k^{\mathsf{f}}$ from the previous computation of the robustness margin, and set the robustness margin to be $\gamma = \gamma_k$. Algorithm 1 is then used on the system matrices $E$, $A^{(\infty)}$, $B$, $C$ by setting in Step 1 the low-rank factors to be $R = Z_k^{\mathsf{f}}$ and $L = Z_k^{\mathsf{r}}$. The rest follows exactly Algorithm 1. The order $r$ of the reduced-order model can be determined by using the criteria for stabilization (13) and the robustness bound (14). This gives the reduced-order system matrices $\widehat{E} = I_r$, $\widehat{A}$, $\widehat{B}$ and $\widehat{C}$.

*Step 3. Construction of the reduced-order controller:* The system matrices of the reduced-order central controller $\widehat{K}$ can then be computed adapting the formulas in (8). First, an approximation to the solutions of the $\mathcal{H}_\infty$-Riccati equations (6) is directly given by

$$\widehat{Y}_{\mathcal{H}_\infty} = W^{\mathsf{T}} E Z_k^{\mathsf{f}} (Z_k^{\mathsf{f}})^{\mathsf{T}} E^{\mathsf{T}} W, \quad \text{and} \quad \widehat{X}_{\mathcal{H}_\infty} = T^{\mathsf{T}} E^{\mathsf{T}} Z_k^{\mathsf{r}} (Z_k^{\mathsf{r}})^{\mathsf{T}} E T,$$

with the low-rank factors $Z_k^{\mathsf{f}}$ and $Z_k^{\mathsf{r}}$ from the computation of the robustness margin, and $W, T$ the truncation matrices from the HINFBT in Algorithm 1. Then, the system matrices of the reduced-order controller are given by

$$\left[ \begin{array}{c|c} -s\widetilde{\widehat{E}} + \widetilde{\widehat{A}} & \widetilde{\widehat{B}} \\ \hline \widetilde{\widehat{C}} & \end{array} \right] = \left[ \begin{array}{c|c} -sI_r + \widehat{A} - (1 - \gamma^{-2})\widehat{Y}_{\mathcal{H}_\infty}\widehat{C}^{\mathsf{T}}\widehat{C} - \widehat{B}\widehat{B}^{\mathsf{T}}\widehat{X}_{\mathcal{H}_\infty}\widehat{Z}_{\mathcal{H}_\infty} & \widehat{Y}_{\mathcal{H}_\infty}\widehat{C}^{\mathsf{T}} \\ \hline -\widehat{B}^{\mathsf{T}}\widehat{X}_{\mathcal{H}_\infty}\widehat{Z}_{\mathcal{H}_\infty} & \end{array} \right] \quad (22)$$

where $\widehat{Z}_{\mathcal{H}_\infty} = (I_r - \gamma^2 \widehat{Y}_{\mathcal{H}_\infty}\widehat{X}_{\mathcal{H}_\infty})^{-1}$.

# 4 Numerical examples

## 4.1 Example setups

We consider the two dimensional flows through a channel with circular obstacles as exemplarily depicted in Figure 1, with controls acting on the boundary of the obstacles, and with observation of locally spatially averaged velocities in a domain of observation downstream of the obstacles.

The generic model then reads

$$\dot{v}(t) + (v(t) \cdot \nabla)v(t) - \frac{1}{\mathsf{Re}}\Delta v(t) + \nabla p(t) = 0, \qquad\qquad \text{in } \Omega, \qquad\qquad (23\text{a})$$

$$\nabla \cdot v(t) = 0, \qquad\qquad \text{in } \Omega, \qquad\qquad (23\text{b})$$

$$\tfrac{1}{\mathsf{Re}}\tfrac{\partial v}{\partial n}v(t) - np(t) = 0, \qquad\qquad \text{on } \Gamma_{\text{out}}, \qquad\qquad (23\text{c})$$

$$v(t) = 0, \qquad\qquad \text{on } \Gamma_w, \qquad\qquad (23\text{d})$$

$$v(t) = ng_{\text{in}}, \qquad\qquad \text{on } \Gamma_{\text{in}}, \qquad\qquad (23\text{e})$$

$$v(t) = ng_i u_i(t), \qquad\qquad \text{on } \Gamma_i, \quad i = 1, 2. \qquad\qquad (23\text{f})$$

Here, $n$ denotes the inward normal of the boundaries, $g_{\text{in}}$ models the inflow boundary condition via a parabola that takes the value 0 at the edges and 2/3 at the center of the inflow boundary, respectively, and $g_i$ and $u_i$ are control shape functions and scalar control value functions. The condition (23c) for the outflow is the standard *do-nothing* condition. The geometrical extensions, the choice of the parameters $u_{\text{in}}$ and $\mathsf{Re}$, and the definition of the output operator $\mathcal{C}$, and of the shape functions are given in the description of the test cases below.

**Test Case 1:** `cylinder wake`

As a first example, we consider the cylinder as it has been described in the benchmark work [39], however in an enlarged domain to reduce the stabilizing effects of the channel walls. To readily include the boundary controls in the Finites Elements discretization, we relax the Dirichlet control conditions (23e) towards Neumann conditions via

$$v(t) = ng_i u_i(t) - \alpha(\tfrac{1}{\mathsf{Re}}\tfrac{\partial v}{\partial n}(t) - np(t)) \text{ on } \Gamma_i, \quad i = 1, 2, \qquad\qquad (24)$$

with a parameter $\alpha$ that is supposed to be small, cf., e.g., [32] for convergence properties of this relaxation in optimal control of stationary flows. The assembling of the associated control operator is explained in [5, Section 9.3].

**Test Case 2:** `double cylinder`

As the second example, we borrow the numerical setup of [17] of the wake of two cylinders in two dimensions; see Figure 3. The actuation of the flow happens through controlled rotation of the individual cylinders. This means we prescribe the control boundary conditions as

$$v\big|_{\Gamma_i} = t_{\Gamma_i} r_i u_i, \quad i = 1, 2, \qquad\qquad (25)$$

where the $\Gamma_i$ are the two boundaries of the cylinders, $t_{\Gamma_i}$ denote the tangential vectors at the boundaries and the $r_i$ the radii, and the $u_i$ are the two scalar input functions, $i = 1, 2$. Although these boundary conditions have no normal component, e.g., $v \cdot n = 0$ at $\Gamma_i$, $i = 1, 2$, and, thus, can be included in a weak formulation with a bounded input operator $\mathcal{B}$ (cp. [4, Sec. 3.1]), we use the same Robin relaxation (24) that is defined to relax controls with normal components.

The spatial discretization is done with $P_2 - P_1$ *Taylor-Hood* finite elements. The input operators are assembled as described in [5, Sec. 9.3] with the penalization parameter $\alpha$ set to $10^{-5}$. Since the output operator $\mathcal{C}$ is of *distributed type*, its assembling with finite elements is straight forward.

We assemble the coefficients of the corresponding linearized system (17) and follow the procedure laid out in Section 3.2 to compute a $\gamma$ and corresponding low-rank approximations to the Gramians defined via (20) and synthesize the (reduced) central dynamical output-based feedback controller via its coefficients

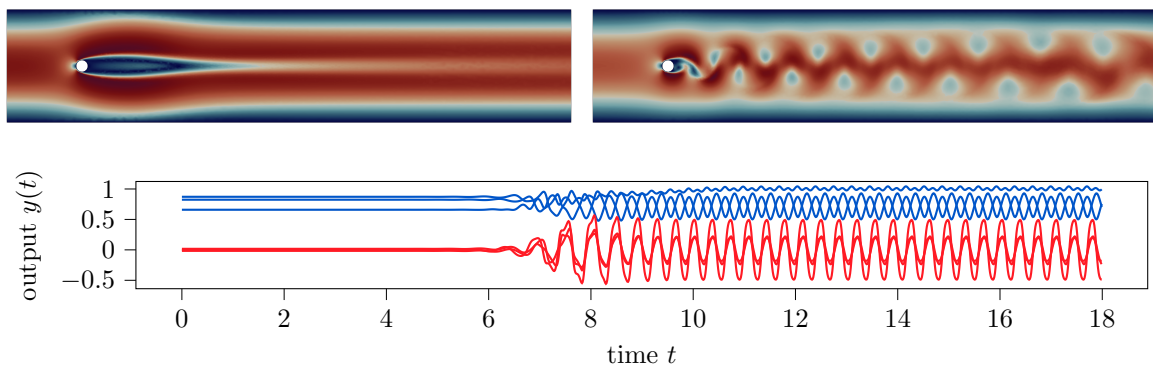$$\widetilde{A}, \ \widetilde{B}, \ \text{ and } \widetilde{C}$$

Figure 2: Example simulation of the cylinder wake with no control input at $\mathsf{Re} = 60$. The plots show the steady state solution (left) and a snapshot of the fully developed time-dependent flow (right) and the measured output signal $y = Cv$ over time $t$. The red lines depict the signal of the lateral averaged velocities, whereas the blue lines depict the measurements of the longitudinal velocities.
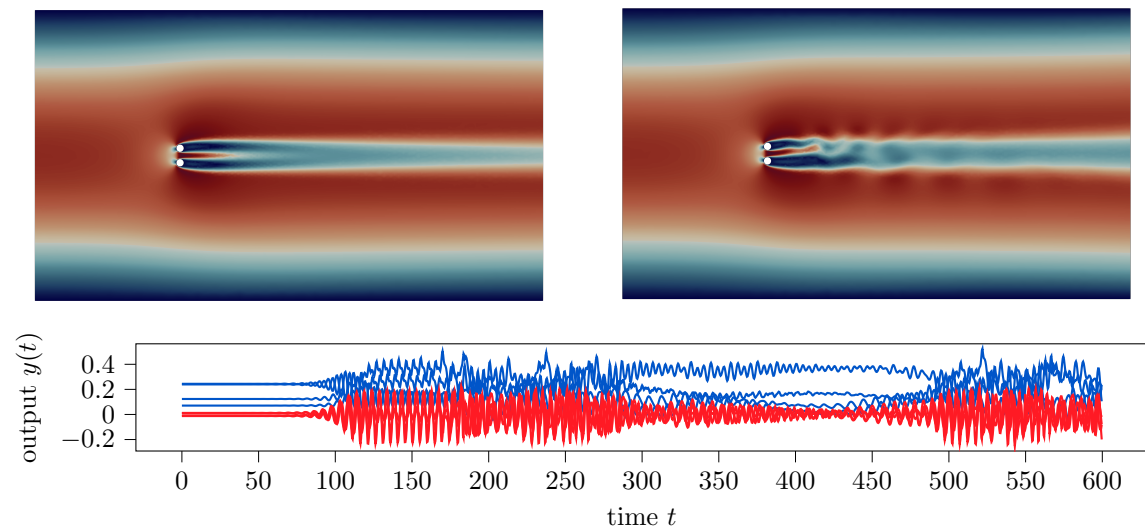


Figure 3: Example simulation of the double cylinder example with no control input at $\mathsf{Re} = 50$. The plots show the steady state solution (left) and a snapshot of the fully developed time-dependent flow (right) and the measured output signal $y = Cv$ over time $t$. The red lines depict the signal of the lateral averaged velocities, whereas the blue lines depict the measurements of the longitudinal velocities.

Table 1: Simulation setups. For the computation of the Reynolds number, $\bar{v} = 1$ is the average inflow velocity and the dynamic viscosity $\nu$ is chosen accordingly.

|  | cylinder wake | double cylinder |
|---|---|---|
| Domain | $[0,5] \times [0,1]$ | $[-20,-20] \times [70,20]$ |
| Obstacles | Circle of radius $r_0 = 0.05$ located at $(0.5, 0.67)$ | Two circles of radius $r_1, r_2 = 0.5$ located at $(0,1)$ and $(0,-1)$ |
| Controls | Outlets at the cylinder periphery at $\pm\frac{\pi}{3}$ of arc length $\frac{\pi}{6}$ | Independent rotation of both cylinders |
| Observation domain | $[2, 2.1] \times [0.3, 0.7]$ horizontally split into 3 equally sized subdomains | $[5,6] \times [-2,2]$ horizontally split into 4 equally sized subdomains |
| Reynolds number | $60 = \frac{1 \cdot 0.05}{\frac{5}{6} 10^{-3}} = \frac{\bar{v} \cdot r_0}{\nu}$ | $60 = \frac{1 \cdot 1}{\frac{5}{3} 10^{-2}} = \frac{\bar{v} \cdot (r_1 + r_2)}{\nu}$ |

Table 2: Simulation parameters.

|  | cylinder wake | double cylinder |
|---|---|---|
| Time interval | $[0, 30]$ | $[0, 300]$ |
| Time step size | $h = 0.00075$ | $h = 0.00390625$ |
| Relaxation parameter | $\alpha = 10^{-5}$ | $\alpha = 10^{-5}$ |
| Dimension of $(v(t), p(t))$ | $(41718, 5418)$ | $(45528, 5809)$ |

as defined in (22). Thus, with $v_\infty$ denoting the target state and linearization point, the closed loop system reads

$$M\dot{v} = A_{\mathsf{S}}v + F(v) + J^\mathsf{T}p + B\widetilde{\widehat{C}}\widetilde{\widehat{x}} + f, \tag{26a}$$

$$0 = Jv + g, \tag{26b}$$

$$\dot{\widetilde{\widehat{x}}} = \widetilde{\widehat{A}}\widetilde{\widehat{x}} + \widetilde{\widehat{B}}C(v - v_\infty). \tag{26c}$$

For the time discretization, we use a uniform grid of size $h$ and employ *backward differencing* of second order in the linear part including the controller and the extrapolation

$$N(v(t+h)) \approx 2N(v(t)) - N(v(t-h))$$

for the nonlinearity. With the initialization of one step of the *Method of Heun*, this results in a time integration scheme of order two.

As the initial value, we use the corresponding steady state $v_\infty$. To trigger the instabilities, we add an input perturbation that acts at the beginning of the simulation like

$$u_\delta = \begin{cases} 10^{-6} \sin(2\pi t), & t \in [0,1] \\ 0, & t > 1. \end{cases}$$

All parameters that define the simulations for both test cases `cylinder wake` and `double cylinder` are listed in Table 2.

## 4.2 Numerical results

The experiments reported here have been executed on a machine with 2 Intel(R) Xeon(R) Silver 4110 CPU processors running at 2.10GHz and equipped with 192 GB total main memory. The computer is run on CentOS Linux release 7.5.1804 (Core).

The solutions to the large-scale Riccati equations (21) were computed using the routines from the M-M.E.S.S. library version 2.0.1 [13,38]. Also, the errors in coprime factorizations have been computed in MATLAB 9.7.0.1190202 (R2019b).

For the spatial discretization, we employ the *FEniCS* [1] Finite Elements toolbox and the python module *dolfin_navier_scipy* [29] to extract the discrete operators for the computation of the feedback gains and for the time integration which is done in *SciPy*.

The code and the raw data of the presented numerical results are available as noted in Figure 4.

Figure 4: Code and Data Availability.

The source code of the implementations used to compute the presented results is available from

<p align="center">doi:10.5281/zenodo.4507759</p>

under the MIT license and is authored by Jan Heiland and Steffen W. R. Werner.

### 4.2.1 Flow stabilization

We investigate the computed controllers in terms of robustness against controller reduction and robustness against linearization errors via the following criteria:

- Does the robustness margin $\gamma$ cover the linearization error, i.e.,

$$\left\| \begin{bmatrix} N - N_\Delta & M - M_\Delta \end{bmatrix} \right\|_{\mathcal{H}_\infty} < \gamma^{-1}$$

  as in (15)?

- Does the robustness margin cover the a-priori estimate for the truncation error, i.e., $\epsilon(\beta + \gamma) < 1$ as in (13)? (For reference, we also check the less conservative a-posteriori estimate $\hat{\epsilon}(\beta + \hat{\gamma}) < 1$ as in (12))

- Does the controller work in the numerical experiment, i.e. does it stabilize the steady state by completely suppressing the oscillations that can be observed in the uncontrolled cases reported in Figure 2 and Figure 3?

To examine the linearization error, we proceed as follows: For the `cylinder wake`, we consider the linearization error that stems from an incomplete iteration for the steady state computation. That is, in (19), instead of the *exact* linearization $A^{(\infty)} = A_{\mathsf{S}} + (\partial_v F)(v_\infty)$ based on the *exact* steady state $v_\infty$, we consider $A^{(\ell)} := A_{\mathsf{S}} + (\partial_v F)(v_\ell)$, where $v_\ell$ is the approximation to $v_\infty$ that is obtained after $\ell$ *Picard* iterations started from the steady state solution for $\mathsf{Re} = 40$.

For the `double cylinder`, we found that at $\mathsf{Re} = 60$, the steady state is so unstable that the *Picard* iteration did not converge. The computation can be done by a *Newton* iteration that, however, does not provide a smooth parametrization of the approximation in the relevant region because of its fast convergence. Therefore, we parametrize the perturbed coefficient $A^{(\ell)} = A_{\mathsf{S}} + (\partial_v F)(v^{(\ell)})$ with $v^{(\ell)}$ as the steady state solution to the problem with the Reynolds number perturbed by $\ell$ thousandths, i.e. $\mathsf{Re}^{(\ell)} = (1 + \frac{\ell}{1000}) \cdot 60$.

Table 3: Coprime factor error of different linearizations for the `cylinder wake` (left) and different Reynolds numbers for the `double cylinder` (right).

| $\ell$ | $\|\Delta^{(\ell)}\|_{\mathcal{H}_\infty}$ | | $\ell$ | $\|\Delta^{(\ell)}\|_{\mathcal{H}_\infty}$ | |
| --- | --- | --- | --- | --- | --- |
| 12 | 1.1113 | | $-96$ | 0.3022 | |
| 24 | 0.0861 | | $-48$ | 0.1540 | |
| 46 | 0.0034 | | $-25$ | 0.0807 | |
| **47** | **0.0029** | $< \gamma^{-1}$ | **$-24$** | **0.0775** | $< \gamma^{-1}$ |
| 48 | 0.0029 | | $-12$ | 0.0389 | |
| 96 | 0.0007 | | $-6$ | 0.0194 | |

We parametrize the truncation error via the truncation threshhold `tol` that defines `tol` $> \sigma_{r+1} \geq \sigma_{r+2} \geq ...$, i.e, the size of those characteristic $\mathcal{H}_\infty$-values that are discarded in Algorithm 1.

We checked the performance in the simulations by examining the empirical variances in the time series of the output signal in the fourth quarter and in the third quarter of the time interval. If the difference between the fourth and third segment was negative, we concluded that the oscillations were on the decline. If the difference was positive but in the order of $10^{-15}$, we concluded that the signals were dominated by numerical errors. In both cases, the corresponding setup was reported as stablizing in the simulation.

In Table 3 we have tabulated the computed error in linearizations and identified the threshhold where $\|\Delta_\ell\| < \gamma^{-1}$.

In Figure 5 we have illustrated the search of the parameter ranges for successful controller setups. For the `cylinder wake`, the estimate precisely confines the range where the controllers are functional. The a-priori estimate (13) turns out to be off the observed failures by a factor of 8, and the estimate on the linearization error by a factor of $2^{1/2}$. Successful stabilization has been observed further outside of the region predicted by the bound with respect to the linearization error and slightly outside the limit defined by the truncation error.

For the `double cylinder`, the picture is less compliant with the predictions. The empirical bound for the truncation error suggested a `tol` of 0.002, which is an underestimate of the stability region by a factor of at least 16 and outside the region that is plotted in Figure 5. The direct computation of the truncation error captured the region much better but was not conservative enough to rule out setups that did not perform. We note that these bounds are designed for the underlying linear system so that such a failure does not contradict the theory. On the other hand, the estimate for the linearization was too conservative by a factor of $2^{3/2}$. Curiously the $\mathcal{H}_\infty$-controller did still perform with a perturbation of the Re number of about 14%. As for the `cylinder wake`, this shows that successful stabilization can be observed outside the region predicted by the linearization error estimates while the error estimates for the truncation error do not leave a margin.

## 5 Conclusions

As illustrated by the numerical examples, the use of the general Riccati-based low-order $\mathcal{H}_\infty$-controller design is well feasible for incompressible flows in simulations. The provided estimates on the guaranteed robustness has been proven reliable though, in some cases, conservative. Together with the theoretical results of earlier works that $\mathcal{H}_\infty$-controller can compensate various model errors, the availability of efficient general purpose numerical methods is key for the applicability of these model-based controllers in simulations and even experiments.
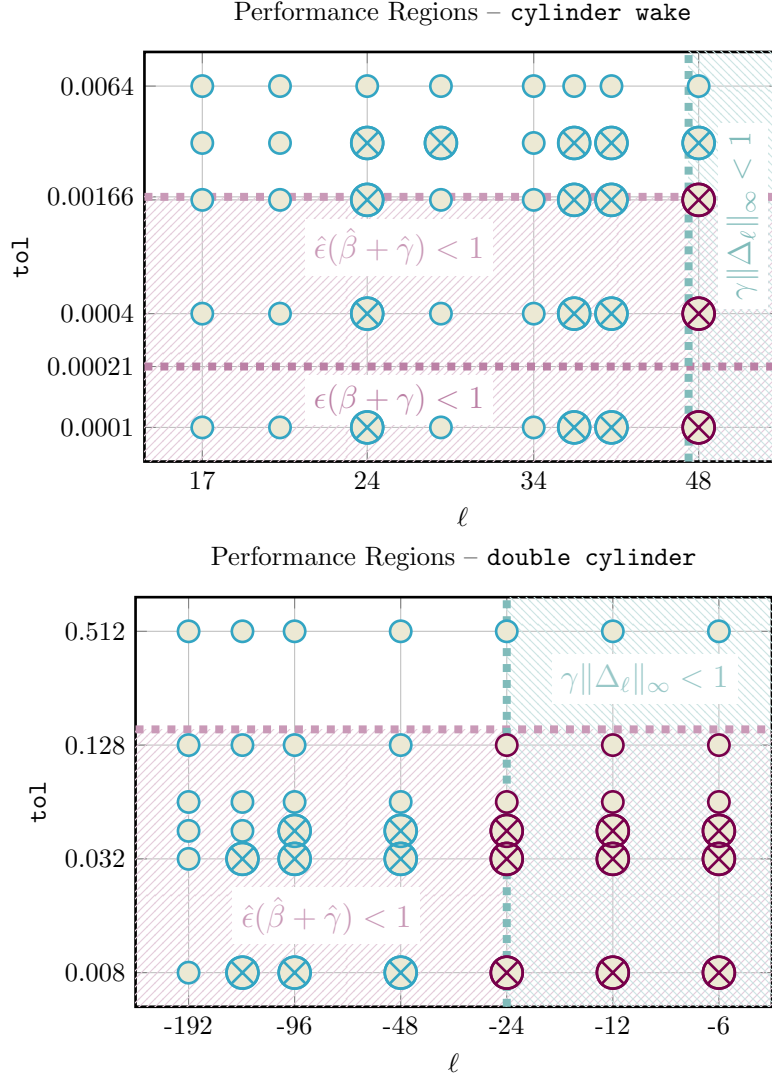
Figure 5: Performance of the controller for different truncation tolerances `tol` and different perturbations levels $\ell$ of the linearization. The symbol $\otimes$ marks the setups for which the controller worked in the experiment and the symbold $\circ$ marks those that failed. The horizontal dashed lines confine the hatched regions in which the stability criterion with respect to the truncation error holds. The vertical lines confines the hatched regions for which the linearization error is within the robustness margin. The intersection of both hatched regions contains those controller setups (marked with red marks) that are predicted as stable by both criteria.

# Acknowledgment

# References

[1] M. S. Alnæs, J. Blechta, J. Hake, A. Johansson, B. Kehlet, A. Logg, C. Richardson, J. Ring, M. E. Rognes, and G. N. Wells. The FEniCS project version 1.5. *Archive of Numerical Software*, 3(100):9–23, 2015. `doi:10.11588/ans.2015.100.20553`.

[2] E. Bänsch, P. Benner, J. Saak, and H. K. Weichelt. Riccati-based boundary feedback stabilization of incompressible Navier-Stokes flows. *SIAM J. Sci. Comput.*, 37(2):A832–A858, 2015. `doi:10.1137/140980016`.

[3] V. Barbu. *Stabilization of Navier-Stokes Flows*. Communications and Control Engineering. Springer-Verlag, London, 2011. `doi:10.1007/978-0-85729-043-4`.

[4] V. Barbu, I. Lasiecka, and R. Triggiani. *Tangential boundary stabilization of Navier-Stokes equations*, volume 181 of *Memoirs of the American Mathematical Society*. AMS, 2006. `doi:10.1090/memo/0852`.

[5] M. Behr, P. Benner, and J. Heiland. Example setups of Navier-Stokes equations with control and observation: Spatial discretization and representation via linear-quadratic matrix coefficients. e-print arXiv:1707.08711, arXiv, 2017. cs.MS, math.DS. URL: `https://arxiv.org/abs/1707.08711`.

[6] D. J. Bender and A. J. Laub. The linear-quadratic optimal regulator for descriptor systems. *IEEE Trans. Autom. Control*, 32(8):672–688, 1987. `doi:10.1109/TAC.1987.1104694`.

[7] P. Benner, Z. Bujanović, P. Kürschner, and J. Saak. RADI: A low-rank ADI-type algorithm for large scale algebraic Riccati equations. *Numer. Math.*, 138(2):301–330, 2018. `doi:10.1007/s00211-017-0907-5`.

[8] P. Benner and J. Heiland. Robust stabilization of laminar flows in varying flow regimes. *IFAC-PapersOnLine*, 49(8):31–36, 2016. 2nd IFAC Workshop on Control of Systems Governed by Partial Differential Equations CPDE 2016, Bertinoro, Italy, 13–15 June 2016. `doi:10.1016/j.ifacol.2016.07.414`.

[9] P. Benner and J. Heiland. Convergence of approximations to Riccati-based boundary-feedback stabilization of laminar flows. *IFAC-PapersOnLine*, 50(1):12296–12300, 2017. 20th IFAC World Congress. `doi:10.1016/j.ifacol.2017.08.2476`.

[10] P. Benner and J. Heiland. Nonlinear feedback stabilization of incompressible flows via updated Riccati-based gains. In *2017 IEEE 56th Annual Conference on Decision and Control (CDC)*, pages 1163–1168, 2017. `doi:10.1109/CDC.2017.8263813`.

[11] P. Benner and J. Heiland. Equivalence of Riccati-based robust controller design for index-1 descriptor systems and standard plants with feedthrough. In *2020 European Control Conference (ECC)*, pages 402–407, 2020. `doi:10.23919/ECC51009.2020.9143771`.

[12] P. Benner, J. Heiland, and S. W. R. Werner. Robust controller versus numerical model uncertainties for stabilization of Navier-Stokes equations. *IFAC-PapersOnLine*, 52(2):25–29, 2019. 3rd IFAC/IEEE CSS Workshop on Control of Systems Governed by Partial Differential Equation CPDE 2019. `doi:10.1016/j.ifacol.2019.08.005`.

[13] P. Benner, M. Köhler, and J. Saak. Matrix equations, sparse solvers: M-M.E.S.S.-2.0.1 – Philosophy, features and application for (parametric) model order reduction. e-print 2003.02088, arXiv, 2020. cs.MS. URL: https://arxiv.org/abs/2003.02088.

[14] P. Benner, J.-R. Li, and T. Penzl. Numerical solution of large-scale Lyapunov equations, Riccati equations, and linear-quadratic optimal control problems. *Numer. Lin. Alg. Appl.*, 15(9):755–777, 2008. doi:10.1002/nla.622.

[15] P. Benner and S. W. R. Werner. MORLAB – Model Order Reduction LABoratory (version 5.0), 2019. see also: http://www.mpi-magdeburg.mpg.de/projects/morlab. doi:10.5281/zenodo.3332716.

[16] M. Bergmann and L. Cordier. Optimal control of the cylinder wake in the laminar regime by trust-region methods and POD reduced-order models. *J. Comput. Phys.*, 227(16):7813–7840, 2008. doi:10.1016/j.jcp.2008.04.034.

[17] J. Borggaard, S. Gugercin, and L. Zietsman. Feedback stabilization of fluids using reduced-order models for control and compensator design. In *2016 IEEE 55th Conference on Decision and Control (CDC)*, pages 7579–7585, 2016. doi:10.1109/CDC.2016.7799440.

[18] R. F. Curtain. A robust LQG-controller design for DPS. *Internat. J. Control*, 79(2):162–170, 2006. doi:10.1080/00207170500512985.

[19] S. Dharmatti, J.-P. Raymond, and L. Thevenet. $H^\infty$ feedback boundary stabilization of two-dimensional Navier-Stokes equations. *SIAM J. Control Optim.*, 49(6):2318–2348, 2011. doi:10.1137/100782607.

[20] J. Doyle, K. Glover, P. P. Khargonekar, and B. A. Francis. State-space solutions to standard $H_2$ and $H_\infty$ control problems. *IEEE Trans. Autom. Control*, 34(8):831–847, 1989. doi:10.1109/9.29425.

[21] J. C. Doyle. Guaranteed margins for LQG regulators. *IEEE Trans. Autom. Control*, 23(4):756–757, 1978. doi:10.1109/TAC.1978.1101812.

[22] B. A. Francis. *A Course In $\mathcal{H}_\infty$ Control Theory*, volume 88 of *Lecture Notes in Control and Information Sciences*. Springer–Verlag, Berlin, 1987. doi:10.1007/BFb0007371.

[23] B. A. Francis and J. C. Doyle. Linear control theory with an $H_\infty$ optimality criterion. *SIAM J. Control Optim.*, 25(4):815–844, 1987. doi:10.1137/0325046.

[24] S. Gugercin, T. Stykel, and S. Wyatt. Model reduction of descriptor systems by interpolatory projection methods. *SIAM J. Sci. Comput.*, 35(5):B1010–B1033, 2013. doi:10.1137/130906635.

[25] M. D. Gunzburger and H. C. Lee. Feedback control of Karman vortex shedding. *J. Appl. Mech.*, 63(3):828–835, 1996. doi:10.1115/1.2823369.

[26] J.-W. He, R. Glowinski, R. Metcalfe, A. Nordlander, and J. Periaux. Active control and drag optimization for flow past a circular cylinder. *J. Comput. Phys.*, 163(1):83–117, 2000. doi:10.1006/jcph.2000.6556.

[27] J. Heiland. A differential-algebraic Riccati equation for applications in flow control. *SIAM J. Control Optim.*, 54(2):718–739, 2016. doi:10.1137/151004963.

[28] J. Heiland. Convergence of coprime factor perturbations for robust stabilization of Oseen systems. e-print arXiv:1911.00983, arXiv, 2019. Submitted to AIMS Mathematical Control & Related Fields. URL: https://arxiv.org/abs/1911.00983.

[29] J. Heiland. dolfin_navier_scipy: a python Scipy FEniCS interface. Github/Zenodo, June 2019. https://github.com/highlando/dolfin_navier_scipy. doi:10.5281/zenodo.3238622.

[30] J. Heiland and E. Zuazua. Classical system theory revisited for turnpike in standard state space systems and impulse controllable descriptor systems. Technical Report 2007.13621, arxiv, 2020. math.OC, Submitted to SIAM Journal on Control and Optimization. URL: http://arxiv.org/abs/2007.13621.

[31] M. Heinkenschloss, D. C. Sorensen, and K. Sun. Balanced truncation model reduction for a class of descriptor systems with application to the Oseen equations. *SIAM J. Sci. Comput.*, 30(2):1038–1063, 2008. doi:10.1137/070681910.

[32] L. S. Hou and S. S. Ravindran. A penalized Neumann control approach for solving an optimal Dirichlet control problem for the Navier-Stokes equations. *SIAM J. Control Optim.*, 36(5):1795–1814, 1998. doi:10.1137/S0363012996304870.

[33] D. L. Kleinman. On an iterative technique for Riccati equation computations. *IEEE Trans. Autom. Control*, 13(1):114–115, 1968. doi:10.1109/TAC.1968.1098829.

[34] D. C. McFarlane and K. Glover. *Robust Controller Design Using Normalized Coprime Factor Plant Descriptions*, volume 138 of *Lect. Notes Control Inf. Sci.* Springer-Verlag, Berlin/Heidelberg, 1990. doi:10.1007/BFB0043199.

[35] J. Möckel, T. Reis, and T. Stykel. Linear-quadratic Gaussian balancing for model reduction of differential-algebraic systems. *Internat. J. Control*, 84(10):1627–1643, 2011. doi:10.1080/00207179.2011.622791.

[36] D. Mustafa and K. Glover. Controller reduction by $\mathcal{H}_\infty$-balanced truncation. *IEEE Trans. Autom. Control*, 36(6):668–682, 1991. doi:10.1109/9.86941.

[37] B. R. Noack, K. Afanasiev, M. Morzyński, G. Tadmor, and F. Thiele. A hierarchy of low-dimensional models for the transient and post-transient cylinder wake. *J. Fluid Mech.*, 497:335–363, 2003. doi:10.1017/S0022112003006694.

[38] J. Saak, M. Köhler, and P. Benner. M-M.E.S.S.-2.0.1 – The Matrix Equations Sparse Solvers library, February 2020. see also: https://www.mpi-magdeburg.mpg.de/projects/mess. doi:10.5281/zenodo.3606345.

[39] M. Schäfer and S. Turek. Benchmark computations of laminar flow around a cylinder. (With support by F. Durst, E. Krause and R. Rannacher). In E. H. Hirschel, editor, *Flow Simulation with High-Performance Computers II. DFG priority research program results 1993-1995*, volume 52 of *Notes Numer. Fluid Mech.*, pages 547–566. Vieweg, Wiesbaden, 1996. doi:10.1007/978-3-322-89849-4_39.

[40] V. Simoncini. Analysis of the rational Krylov subspace projection method for large-scale algebraic Riccati equations. *SIAM J. Matrix Anal. Appl.*, 37(4):1655–1674, 2016. doi:10.1137/16M1059382.

[41] V. Simoncini, D. B. Szyld, and M. Monsalve. On two numerical methods for the solution of large-scale algebraic Riccati equations. *IMA J. Numer. Anal.*, 34(3):904–920, 2014. doi:10.1093/imanum/drt015.

[42] H.-S. Wang, C.-F. Yung, and F.-R. Chang. Bounded real lemma and $H_\infty$ control for descriptor systems. *IEE Proceedings - Control Theory and Applications*, 145(3):316–322, 1998. doi:10.1049/ip-cta:19982048.

[43] H. K. Weichelt. *Numerical Aspects of Flow Stabilization by Riccati Feedback*. Dissertation, Otto-von-Guericke-Universität, Magdeburg, Germany, 2016. `doi:10.25673/4493`.

[44] C. H. K. Williamson. Vortex dynamics in the cylinder wake. *Annual Review of Fluid Mechanics*, 28(1):477–539, 1996. `doi:10.1146/annurev.fl.28.010196.002401`.

[45] G. Zames. Feedback and optimal sensitivity: Model reference transformations, multiplicative seminorms, and approximate inverses. *IEEE Trans. Autom. Control*, 26(2):301–320, 1981. `doi:10.1109/TAC.1981.1102603`.

[46] K. Zhou, J. C. Doyle, and K. Glover. *Robust and Optimal Control*. Prentice-Hall, Upper Saddle River, NJ, 1996.